Holographic Optical Switching: The "ROSES" Demonstrator

W. A. Crossland, I. G. Manolis, M. M. Redmond, K. L. Tan, T. D. Wilkinson, M. J. Holmes, T. R. Parker, H. H. Chu, J. Croucher, V. A. Handerek, S. T. Warr, B. Robertson, I. G. Bonas, R. Franklin, C. Stace, H. J. White, R. A. Woolley, and G. Henshall

Abstract—The design, assembly, and performance of a prototype 1×8 free-space switch demonstrater using reconfigurable holograms are reported. Central to the switch fabric is a ferroelectric liquid crystal (FLC) on silicon spatial light modulator (SLM) deposited with a 540×1 array of highly reflective and planar mirror strips. The input and output ports of the switch are fabricated as a linear array of silica planar waveguides connected to single-mode fibers, and the holographic beam-steerer operates without the need for adjustment or dynamic alignment. The waveguide array and the single Fourier transform lens for the $2f$ holographic replay system are housed in an opto-mechanical mount to provide stability. The switch operates at 1.55 μm wavelength and has a designed optical bandwidth of $>$60 nm. The first measured insertion loss and crosstalk figures are 16.9 dB and $-$19.1 dB, respectively. Improvements in SLM performance, the use of new addressing schemes and the introduction of better alignment techniques are expected to improve these figures considerably. The preliminary performance of a 3×3 optical crossconnect is also presented to show that this technology is scalable to $N \times N$ switching fabrics.

Index Terms—Ferroelectric liquid crystal, optical crossconnect, optical switch, reconfigurable hologram, spatial light modulator, waveguide.

I. INTRODUCTION

THE rapidly evolving demands of telecommunications and avionics systems have created a new market for high-capacity all-optical photonic switches. The scale of the networks proposed leads ultimately to requirements for very large switching fabrics (e.g., $>1 \times 32$ and $>64 \times 64$). Currently, there are several different technologies being developed to implement such systems, including thermo-optic waveguide (TOW) switches [1], mechanical switches, and micro-electro mechanical systems (MEMS) [2]. An alternative approach potentially capable of realising such systems uses holographic optical beam deflectors based on binary and multiple-phase liquid crystal spatial light modulators [3]. These are moderate speed, optically transparent, switches capable of handling any data format or bit rate. In addition, as the light is deflected through free-space, multiple signal beams can be simultaneously interconnected allowing the switch to be scaled up to hundreds of channels. Such switches are ideally suited to applications in network protection and restoration after failure, dynamic connection provisioning, and polling networks of optical sensors.

In this paper, the design and operation of a 1×8 free-space holographic optical switch developed for sensor polling will be described. In addition, in order to show that this technology is scalable to $N \times N$ switches, the preliminary results for a bench top 3×3 switch will also be presented.

The 1×8 switch uses a hologram recorded onto a ferroelectric liquid crystal over silicon spatial light modulator (FLC/Si SLM) [3], [4] to steer the incoming beam to the desired output port [5]. The binary FLC is ideally configured as a reflective half-wave plate. FLCs have been shown to record binary-phase holograms [6] and to replay lossy binary phase holograms without polarization sensitivity regardless of the wave-plate thickness and FLC switching angle [7]. A previous free-space optical switch demonstration using FLC on glass holograms in a $4f$ transmissive bench set-up has been reported [8]. The ROSES [9], [10] switch demonstrator uses a reflective FLC/Si SLM as the hologram recording device; a waveguide array (WGA) to provide the input and output ports, and a custom-made opto-mechanical mount with six-axis alignment adjusters to house the WGA, a single collimation/transform lens, and the SLM.

Although prototype photonic switches have already been demonstrated using thermo-optic waveguide and MEMS-based technologies, it is believed that holographic beam deflecting switches offer a more scalable and reliable approach to producing high-capacity all-optical photonic switches. Thus, throughout this paper the advantages and challenges associated with this technology will be discussed and compared against these competing technologies.

II. DESIGN OF ROSES SWITCH

A. Operation of Switch

The primary aim of the ROSES project was to develop the technology required to implement a large scale $N \times N$ holographic beam deflecting switch. As a first step toward this goal, a prototype polarization independent linear 1×8 fiber optic routing switch has been demonstrated. The switch was designed
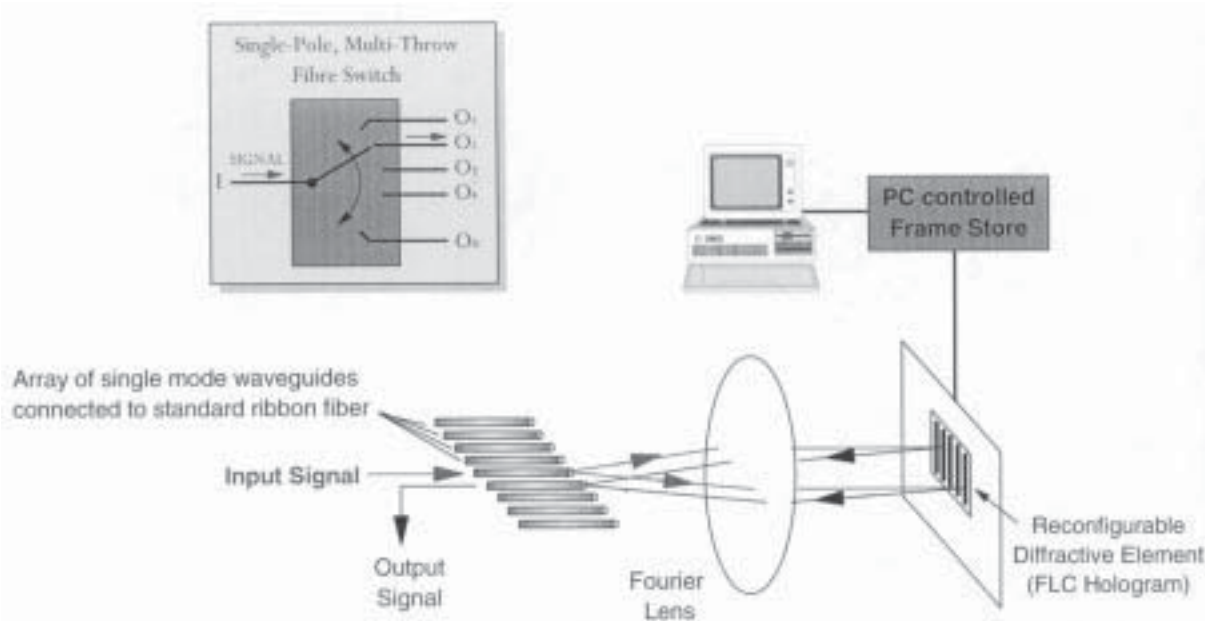
Fig. 1.   Operation of the ROSES 1×8 holographic routing switch. SLM deflects signal beam through an angle φ dependent on period of hologram. Can control which output port light is diffracted into.

to take a signal beam from a single-mode fiber, and dynamically route it to one of eight single-mode output fibers. The switch is shown schematically in Fig. 1, and consists of four main components: a waveguide array providing spatial fan-in to and from the input and output fibers; a Fourier lens, a reflective binary-phase ferroelectric liquid crystal silicon backplane SLM that acts as a beam-steering element, and a custom interface board. The Fourier lens was a commercially available component, while the silicon backplane and silica-on-quartz waveguide array were custom-designed within the project and fabricated at external foundries. Custom optomechanics were used to align and control the relative positions of all optical components. In addition, the optomechanics, ribbon fiber connectors and electronic interface board were all mounted on a common aluminum baseplate.

The basic operation of the switch is as follows: the optical signal is launched down the input fiber, and couples via a connector into the ribbon fiber. The signal then couples into the input waveguide and propagates to the launch end of the waveguide array, from where it is collimated (Fig. 1) by the Fourier lens onto the SLM. The SLM acts like a phase-only diffraction grating with a tuneable period and pattern, creating a deflection angle, ϕ, of the reflected beam. By controlling the deflection angle, the beam may be made to return to a selected point on the waveguide array, and hence couple into the chosen output waveguide. The output signal then propagates across the waveguide array and into the ribbon fiber and output fiber. The deflection angle depends on the phase modulation pattern (the hologram), which is downloaded from a PC via an electronic interface board. The maximum deflection angle for 20 μm pixels is 2.22° at 1550 nm.

Due to the binary-phase nature of the hologram, light is diffracted symmetrically into both the +1 and −1 orders. The

channels were to the left of the input channel, and the 2nd, 4th, 6th, and 8th channels were to the right of the input waveguide, as shown in Fig. 1). In order to minimize crosstalk caused by the unwanted symmetric order, the waveguide was designed with the unwanted orders landing between the output waveguides.

B. The Liquid Crystal over Silicon (LCOS) Spatial Light Modulator

The SLM consists of a linear array of 540 pixellated electrodes, each 18 μm $\times$ 6 mm, with a 2 μm dead space between the pixels (Fig. 2). On the silicon backplane, each pixel is connected to an integrated SRAM pixel drive circuit and suitable access circuitry to which the required hologram patterns were down-loaded from a custom interface board (the PC controlled frame store shown in Fig. 1). An extra silicon-processing step was carried out within the project, to lay down a layer of optical quality aluminum "mirror" over the pixels [11]. Light incident on the SLM passes through a layer of birefringent liquid crystalline material [12] with an optical axis orientation controlled by the voltage applied to the pixel. It is then reflected from the aluminum mirror and passes back through the liquid crystal layer. The first-order diffraction efficiency of a binary-phase hologram with FLC layer thickness d, and molecular tilt angle θ is given by (1), where Δn is the birefringence and λ is the operating wavelength [7]

$$\eta = \sin^2 2\theta \sin^2\left(\frac{2\pi\Delta n d}{\lambda}\right). \tag{1}$$

Equation (1) shows that efficiency is maximized when the device acts as a half-wave plate in reflection at the wavelength of operation (1550 nm), and the ferroelectric tilt angle is 45°. Hence, we aimed to use high tilt FLC materials.
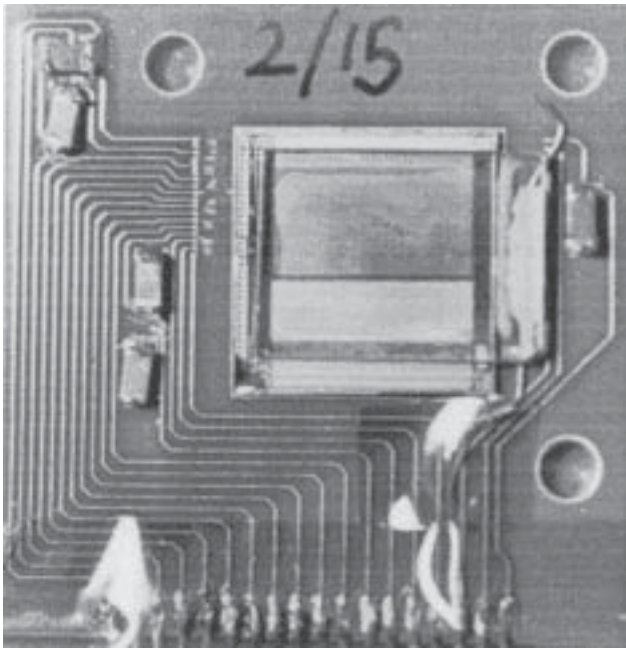
Fig. 2.   Photograph of the assembled SLM.

the FLC phase sequence and this has implications on the alignment properties of the material. Firstly, the absence of a Sa phase means that on cooling into the Sc* phase [12] two equivalent orientations of the smectic layers appear so that, in order to achieve a monodomain, one of the two must be selected by suitable alignment techniques. Secondly, once the monodomain is obtained one of the two-switched states is preferred to the other and so the material is monostable not bistable, which is a disadvantage from the point of view of addressing schemes. Also, since the orientational viscosity of an FLC material typically increases with increased tilt angle, high tilt angle FLC materials tend to exhibit lower operational speeds than standard FLC materials for the same applied electric fields. However, in comparison with standard FLC materials, high tilt angle FLCs exhibit a tilt angle, which is fairly temperature independent. Hence, a device using a high tilt FLC should have an efficiency which is much less temperature sensitive and hence possess a broader operational temperature range.

Operation at telecom wavelengths also has implications on the device performance. Firstly, in order to achieve a half wave plate thickness at 1550 nm the SLM thickness must be approximately three times that required for visible wavelengths. Secondly, at telecoms wavelengths, the birefringence of the FLC may be less than that at visible wavelengths. Again this would necessitate the use of a thicker FLC layer to maximize the diffraction efficiency. Our SLM was fabricated using a fixed voltage active silicon backplane and hence increases in the cell thickness results in a decrease in the available applied electric field, and correspondingly a decrease in the speed of response of the FLC.

We selected two FLC materials:—CS2005 [14] a commercially available high tilt angle compound with a phase sequence I-(73)-N*-(65)-Sc*-(−19)-Cr and a tilt of 43° at room temper-

and a tilt angle of 34° at room temperature. We subjected them to fields of up to 10 V/μm at frequencies of approximately 1–2 kHz with a small dc offset (a few mV) at temperatures just below their I-Sc* and N*-Sc* phase transition temperatures in order to obtain monodomains. In addition we were able to rotate the layer orientation of the monodomain achieved in CDRR8 using asymmetric fields and thus obtain bistable operation [16]. Characterization of the performance of both compounds confirmed that, at fields currently available to us from our silicon active backplane, trade-offs have to be made between the speed of response of the device and its efficiency when selecting a suitable FLC. Thus we chose CDRR8 for our $1 \times N$ demonstrator device and CS2005 for our $N \times N$ switch [17]. The $N \times N$ switch is based on all glass SLMs using ITO electrodes, which allow higher operational fields to be applied to the FLC and permit us to demonstrate the relatively high efficiencies which can be obtained in binary SLMs using FLC materials with tilt angles approaching 45°.

C. Hologram Design

The hologram refers to the phase modulation pattern and period applied by the SLM. In practice, the effect of the phase modulation is to split the beam incident on the SLM into a number of reflected beams, each corresponding to a different diffraction order of the phase modulation. Only one of these diffraction orders is created intentionally: the others are unwanted. The intended diffraction order carries the signal into the selected output waveguide, while the unwanted diffraction orders, unless controlled and positioned appropriately, can lead to crosstalk and back reflection. The output angle of each diffraction order, measured from the optical axis is given by (2), where Λ is the period of the phase modulation, usually known as the hologram period, and m is an integer that identifies a particular diffraction order.

$$\sin \phi_{\text{OUT}} = \sin \phi_{\text{IN}} + \frac{m\lambda}{\Lambda}. \qquad (2)$$

As illustrated previously in Fig. 1, the SLM is pixellated, and so the possible hologram periods must be an integer multiple of the pixel pitch. On arriving at the launch end of the waveguide array, the tails of the beams in the unwanted diffraction orders will couple into their nearest waveguides, leading to crosstalk. Of particular concern are the zeroth-order reflection ($m = 0$: at angle of incidence = angle of reflection) and also the order symmetric to the one used for switching (same value of $|m|$, opposite sign), since for binary phase modulation as provided on the demonstrator SLM, these orders cannot be eliminated. The hologram patterns were calculated using Fourier series analysis under the constraint of suppressing crosstalk from unwanted diffraction orders to an acceptable level: the targets for total crosstalk were −20 dB, and total backreflection below −40 dB. The number of pixels used to display the phase modulation was chosen to be sufficient to avoid excess crosstalk and insertion loss penalties due to clipping of the tails of the beam incident on the SLM. The theoretical diffraction efficiency of the holograms varies between 4 dB and 4.8 dB: 4 dB of this is inherent to

TABLE I
REQUIRED WAVEGUIDE ALIGNMENT TOLERANCES AND PERFORMANCE OF OPTOMECHANICS

Waveguide Parameter	Required Tolerance	Optomechanics Performance	Range
x-lateral position	±0.2μm	±0.5μm	±1mm
y-lateral position	±1.3μm	±0.5μm	±1mm
z-lateral position	±10μm	±0.5μm	±0.5mm
Rotation about x-axis	±6mrad	±0.025mrad	±50mrad
Rotation about y-axis	±4mrad	±0.025mrad	±50mrad
Rotation about z-axis	±25mrad	±0.05mrad	±25mrad

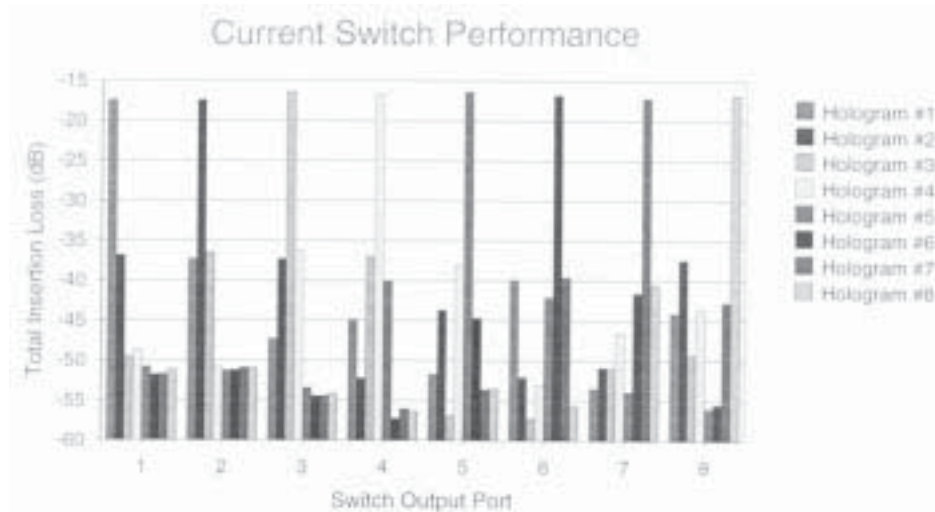Fig. 3.   ROSES 1×8 switch performance (input power of 1 mW at 1550 nm).

suppress crosstalk from unwanted diffraction orders. Additionally, in order to maintain electro-chemical stability of the FLC, the pixels were DC balanced by scrolling the hologram pattern (one pixel at a time) across the SLM.

D. Waveguide Array

A waveguide array was used to provide spatial fan-in in order to increase the wavelength range per port, while avoiding the need for microlenses. The waveguide index and cross-section were optimized to maximize the wavelength range of the system for a given crosstalk specification, including the effect of lens aberrations (assuming perfect alignment), and subject to the constraint of acceptable coupling losses to external ribbon fiber. The waveguide array was designed to provide a 1 dB optical bandwidth of 60 nm. In perfect alignment, the theoretical 1 dB bandwidth is 79 nm, which would increase to 89 nm with a custom lens.

E. Optomechanics

The full range of alignment tolerances was analyzed, with the most severe being that of the transverse position of the waveguide array, with sub-micron accuracy required to maintain the required wavelength range. A custom-made optomechanical mount was procured with six-axis alignment adjusters to hold the waveguide array (glued to a waveguide carrier), the

optomechanics. In use the device has no moving parts and the deflection angle produced by the beam deflector only depends on the binary pattern presented on the FLC SLM. No dynamic alignment is required.

III. PERFORMANCE OF SWITCH

In order to determine the capabilities of the system, the optical insertion loss, crosstalk, wavelength response, and temporal response of the switch were experimentally investigated. The first step in testing the full switch involved accurately aligning the waveguide with respect to the signal beams. Once this was completed, the SLM was configured to direct light into each of the output channels in turn and power measurements made to determine the full 8×8 crosstalk matrix (power diffracted into the signal channels and corresponding crosstalk into the other channels). Due to the slow response time of the power meter compared to the hologram update rate (100 frames/s), the optical signals were time-averaged. The results of these measurements are shown in Fig. 3. For some switch configurations there was a noticeable fluctuation in the crosstalk power of up to ±0.25 dB, although this was not the case for the signal beam (signal power coupled into the required output waveguide), which remained extremely stable and had a measurement error of better than ±0.1 dB.

4 dB loss due to the binary-phase nature of the hologram, a 0.66 dB loss due to the nonideal liquid crystal tilt angle of the material used (CDRR8), and a dead space loss of 0.92 dB. The calculation assumes a perfect cell thickness and no absorption loss in the device. In order to determine whether the SLM had been perfectly fabricated, a separate test rig was set up to measure the diffraction efficiency (defined as the ratio of power in the $+1$ order when a binary-phase hologram is displayed to the power in the zeroth-order when no hologram is displayed) and real efficiency of the device (defined as the ratio of power in the $+1$ order to the incident power). The diffraction efficiency for channel eight was measured to be 18.1% (7.4 dB loss). This difference between this value and the ideal figure of 5.6 dB is due primarily to an nonoptimized cell thickness, and may be corrected for by fine-tuning the cell width. The real efficiency, which takes into account absorption within the SLM was found to be $8.0 \pm 0.2\%$, giving the device an overall loss of 11.0 ± 0.1 dB. Measurements of the ITO coated coverplate showed that this excess loss was almost entirely due to absorption in the ITO layer, a problem that can easily be corrected for by using a thinner layer of this material.

The maximum theoretical insertion loss for an ideally aligned switch should be of the order of 9.4 dB. This assumes a perfectly optimized, nonabsorbing SLM, lens aberration losses of 0.6 dB, and measured propagation losses through the waveguide and connectors of 2.4 dB. In addition, there is a variation in efficiency between the various grating designs of 0.8 dB due to the optimization of certain hologram patterns to minimize crosstalk between channels. Thus, the minimum insertion loss is 8.6 dB and the maximum insertion loss is 9.4 dB (average 9.0 ± 0.4 dB). Taking into account the real efficiency of the SLM, measured to be 11.0 ± 0.1 dB, we obtain an average theoretical insertion loss of 14.4 ± 0.5 dB.

After the switch was aligned, the full 8×8 crosstalk matrix was measured. The insertion loss of the switch was found to be 16.9 ± 0.5 dB, which compares relatively well with the predicted average loss of 14.4 ± 0.5 dB. The excess 2.5 dB loss may be accounted for by a number of mechanisms including nonoptimum alignment, increased aberrations introduced by misalignment, beam distortion due to a nonuniform curvature of the SLM and nonuniform cell thickness, and the presence of dead pixels. The variation of insertion loss across all eight channels was measured to be only ± 0.5 dB. By comparison, the theoretical variation in hologram diffraction efficiency was calculated to be ± 0.4 dB. The signal-to-peak noise crosstalk varied between a worst case of -19.1 dB to optical isolations as high as -40.5 dB. These results are extremely promising, as the target crosstalk figure was -20 dB and the theoretical worst crosstalk figure was calculated to be -21.0 dB. The fact that the crosstalk failed to meet specifications may again be accounted for by misalignment. If excess aberrations (caused by a nonuniform SLM or a tilt in the system) are present, the beam size will increase and light from the symmetric diffraction order will spill over into the wrong output channel. Finally, it should be noted that in the case of a $N \times N$ cross-connect, theoretical crosstalk values below -40 dB are possible. This will be discussed in the following section.

TABLE II
THEORETICAL LOSS FIGURES FOR SLM AND SWITCH

Parameter	Loss
Binary-phase efficiency	4dB
Non-ideal liquid crystal tilt angle	0.66dB
Dead space loss	0.92dB
Theoretical SLM efficiency	**5.6dB**
Worst case variation in hologram efficiency	0.8dB
Lens aberrations for perfect alignment	0.6dB
Measured two way propagation loss through external connector and waveguide array	2.4dB
Theoretical maximum loss	**9.4dB**

frames/s). Thus in order to monitor the temporal stability of the switch, the output from each signal channel was monitored using a photodiode and digital oscilloscope. The temporal variation in the power launched down each signal waveguide was found to be relatively small, with the measured voltage varying between $\pm 3.6\%$ and $\pm 5.3\%$ of the average signal. The biggest dip occurred at the start of each new hologram frame. This result shows that the hologram update scheme used in the system (scrolling the pattern one pixel at a time) does not unduly interrupt the optical signal being sent through the switch. In addition, the wavelength response of the switch was measured as having an insertion loss variation of 1.3 dB over a 30 nm range and 3 dB over a 60 nm range (centered at 1520 nm). The limited bandwidth of the switch, and the offset of the minimum insertion loss from 1550 nm to 1520 nm was due to alignment errors, an error in the focal length of the lens, and a rotation of the waveguide with respect to the signal beams. The actual central operating wavelength can be adjusted for by optimizing the position of the output waveguides and hologram patterns. Finally, the back reflection from the switch was investigated and a worst case value of -35.1 dB was measured.

Considering the preliminary nature of these measurements, and the on-going development of the SLM, and alignment procedures, the switch performance results presented in this section are quite encouraging. It is expected that the switch performance will improve significantly as SLM devices more precisely optimized for 1550 nm are made available, better addressing schemes are implemented, and more alignment experience is gained. In particular, the use of thinner ITO layers and optimization of the SLM cell thickness should reduce the average insertion loss to well below 10 dB.

IV. $N \times N$ OPTICAL SWITCH

One of the main aims of the ROSES project was to develop the technology required to implement a large-scale $N \times N$ holographic optical crossconnect. An $N \times N$ channel switch can be built using a single SLM, however, the fan in to the output fibers limits scalability and performance. A well-known solution to this problem is to build a holographic switch using two arrays of sub-holograms, as shown in Fig. 4 [5], [8]. This ar-

DOCKET ALARM

Explore Litigation Insights

Docket Alarm provides insights to develop a more informed litigation strategy and the peace of mind of knowing you're on top of things.

Real-Time Litigation Alerts

Keep your litigation team up-to-date with **real-time alerts** and advanced team management tools built for the enterprise, all while greatly reducing PACER spend.

Our comprehensive service means we can handle Federal, State, and Administrative courts across the country.

Advanced Docket Research

With over 230 million records, Docket Alarm's cloud-native docket research platform finds what other services can't. Coverage includes Federal, State, plus PTAB, TTAB, ITC and NLRB decisions, all in one place.

Identify arguments that have been successful in the past with full text, pinpoint searching. Link to case law cited within any court document via Fastcase.

Analytics At Your Fingertips

Learn what happened the last time a particular judge, opposing counsel or company faced cases similar to yours.

Advanced out-of-the-box PTAB and TTAB analytics are always at your fingertips.

API

Docket Alarm offers a powerful API (application programming interface) to developers that want to integrate case filings into their apps.

LAW FIRMS

Build custom dashboards for your attorneys and clients with live data direct from the court.

Automate many repetitive legal tasks like conflict checks, document management, and marketing.

FINANCIAL INSTITUTIONS

Litigation and bankruptcy checks for companies and debtors.

E-DISCOVERY AND LEGAL VENDORS

Sync your system to PACER to automate legal marketing.

fastcase®
Smarter legal research.